Design and Open-Loop Control of the ParkourBot, a Dynamic Climbing Robot

Amir Degani, *Member, IEEE*, Andrew W. Long, Siyuan Feng, H. Benjamin Brown, Robert D. Gregg, *Member, IEEE*, Howie Choset, Matthew T. Mason, *Fellow, IEEE*, and Kevin M. Lynch, *Fellow, IEEE*

***Abstract*—The ParkourBot climbs in a planar reduced-gravity vertical chute by leaping back and forth between the chute's two parallel walls. The ParkourBot is comprised of a body with two springy legs and its controls consist of leg angles at touchdown and the energy stored in them. During flight, the robot stores elastic potential energy in its springy legs and then converts this potential energy in to kinetic energy at touchdown, when it "kicks off" a wall. This paper describes the ParkourBot's mechanical design, modeling, and open-loop climbing experiments. The mechanical design makes use of the BowLeg, previously used for hopping on a flat ground. We introduce two models of the BowLeg ParkourBot: one is based on a nonzero stance duration using the spring-loaded inverted pendulum model, and the other is a simplified model (the simplest parkour model, or SPM) obtained as the leg stiffness approaches infinity and the stance time approaches zero. The SPM approximation provides the advantage of closed-form calculations. Finally, predictions of the models are validated by experiments in open-loop climbing in a reduced-gravity planar environment provided by an air table.**

***Index Terms*—Climbing robots, dynamic locomotion, legged robots, mechanism design.**

I. Introduction

A. Parkour and the ParkourBot

THIS study is inspired in part by the grace, efficiency, and adaptability of human parkour, also known as free running. Parkour is the art of moving from place to place as quickly and efficiently as possible, overcoming obstacles using leaps, swings, rolls, and other dynamic movements, whereas walls, chutes, and trenches are obstacles that may not be navigable using less dynamic forms of locomotion; in parkour these "obstacles" are potential sources of reaction forces for a well-placed hand or foot. For parkour practitioners (traceurs) to make maximum use of these handholds and footholds, they must have precise control of their body. By taking advantage of dynamics, and by knowing the geometry and contact properties (e.g., friction and restitution) of the environment, the set of reachable states by parkour is vastly increased over that by more conventional locomotion.

To proceed efficiently over obstacles, the traceur continuously redirects momentum and transfers potential energy (muscles and tendons) to kinetic energy and vice versa. Inspired by parkour, in this paper we introduce the biped *ParkourBot*, which climbs and descends in a planar reduced-gravity vertical chute by leaping back and forth between the chute's two parallel walls (see Fig. 1). The ParkourBot stores elastic potential energy in its springy legs during flight, then converts this potential energy in to kinetic energy when it "kicks off" a wall.

The ParkourBot is based on two dynamic robots we previously built. The first, the BowLeg hopper [1], [2], is a monopod with high energy efficiency that requires feedback for stable hopping on the horizontal ground. The second, the dynamic single-actuator climber (DSAC) [3], [4], sacrifices energy efficiency for stable open-loop climbing of a chute. This paper

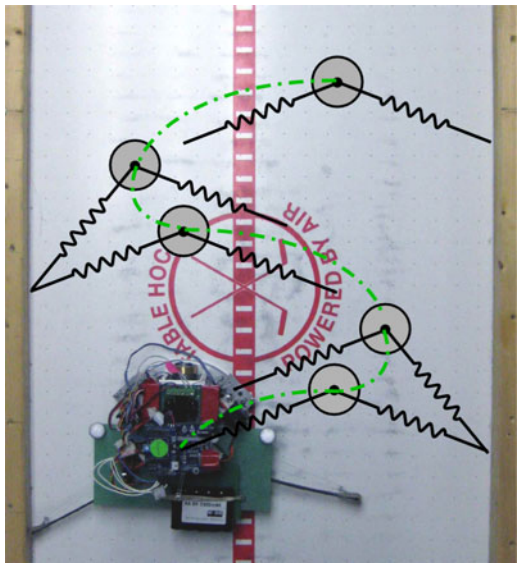

Fig. 1. ParkourBot and a graphical depiction of its climbing motion using the SLIP model. The ParkourBot moves on an inclined air table, providing a reduced gravity, planar environment.

Manuscript received April 9, 2013; revised October 2, 2013; accepted January 12, 2014. Date of publication January 29, 2014; date of current version June 3, 2014. This paper was recommended for publication by Editor A. Kheddar upon evaluation of the reviewers' comments. This work has been supported in part by the National Science Foundation under Grant IIS-08030826 and Grant IIS-0803734. This work was also partially supported by a grant from the German-Israeli Foundation for Scientific Research and Development.

A. Degani is with the Faculty of Civil and Environmental Engineering, Technion, Haifa 32000 Israel (e-mail: adegani@technion.ac.il).

A. W. Long and K. M. Lynch are with the Department of Mechanical Engineering and the Northwestern Institute on Complex Systems, Northwestern University, Evanston, IL 60208 USA (e-mail: awlong@u.northwestern.edu; kmlynch@northwestern.edu).

S. Feng, H. B. Brown, H. Choset and M.T. Mason are with the Robotics Institute, Carnegie Mellon University, Pittsburgh, PA 15213 USA (e-mail: sfeng@cs.cmu.edu; hbb@cs.cmu.edu; choset@cs.cmu.edu; matt.mason@cs.cmu.edu).

R. D. Gregg is with the Departments of Mechanical Engineering and Bioengineering, University of Texas, Richardson, TX 75080 USA (e-mail: rgregg@ieee.org).

This paper has downloadable supplementary multimedia material of ParkourBot robot design, experimental setup, and open-loop experiments, available at http://ieeexplore.ieee.org.

Color versions of one or more of the figures in this paper are available online at http://ieeexplore.ieee.org.

Digital Object Identifier 10.1109/TRO.2014.2300213

describes the design and control of the biped BowLeg ParkourBot that inherits properties of the BowLeg hopper and the DSAC. The ParkourBot is designed to address different types of climbing tasks such as simple chutes and more complex environments having footholds at different orientations. This paper focuses on climbing between two vertical walls with demonstrations in a planar reduced-gravity environment.

B. Contributions

This paper describes the first robot capable of dynamically climbing and descending between two parallel vertical walls, in reduced gravity, by leaping back and forth. This is our first step toward dynamic navigation of complex vertical environments with footholds at different orientations. We describe the mechanical design of the robot and two simplified models of the robot's dynamics: the spring-loaded pendulum (SLIP) model and the "simplest parkour model" (SPM). The SLIP model assumes a springy leg of finite stiffness, giving rise to a nonzero duration stance phase requiring numerical integration of the equations of motion.[1] The SPM approximates the leg as infinitely stiff, giving rise to an instantaneous stance phase with equations of motion that can be solved analytically, an attractive simplification for future real-time motion planning. The controls to the models are the leg angle at impact and the amount of potential energy converted to kinetic energy when the leg kicks off the wall.

Using these two models, we demonstrate the existence of open-loop stable climbing and descending gaits using constant control inputs. Experiments with two models of the ParkourBot show that the simplified models provide a reasonable approximation to the actual dynamics. Finally, we demonstrate successful implementation of open-loop stable climbing between two vertical walls in the reduced-gravity environment provided by an inclined air table.

This paper extends our previous work in [5] and [6] by combining and comparing two models, the SLIP model and the SPM, and providing new analytical results for each. We find qualitative agreement between the SLIP model and the SPM's predictions of local stability and BOA. We validate that the SPM retains the qualitative behavior of the SLIP model, and that both models are representative of our experimental results. Furthermore, we show period-doubling bifurcation plots matching open-loop experiments.

C. Outline of the Paper

We begin by reviewing related work in Section II. In Section III, we describe the mechanical design of the ParkourBot. Section IV describes the two models of the ParkourBot, the SLIP model and the SPM, and examines the relationship between these models as well as their fixed points and other features. In Section V, we provide results of experiments on ParkourBots at Carnegie Mellon University and Northwestern University. These results qualitatively agree with the predictions of the SLIP model and the SPM, and demonstrate successful open-loop climbing and descending in a chute on an air table providing a reduced gravity, planar environment. We conclude with discussion in Section VI and directions for future work in Section VII.

[1] In this study, the pendulum is not technically "inverted" relative to gravity during stance, but we retain the term "SLIP" to draw analogy to previous work on horizontal running using a similar model of a mass–spring pendulum.

II. Related Work

This study is related to previous work on dynamically locomoting robots, particularly hopping, passive dynamic walking, and running robots, with many legs or as few as one. The work of Raibert *et al.* is particularly influential, as it demonstrated that simple control laws could be used to stabilize hopping and controlling the running speed and direction of 2-D and 3-D single-leg hoppers [7], [8].

To improve the energy efficiency of a hopping robot, Brown and Zeglin introduced the single-leg BowLeg Hopper, which can traverse a series of stepping stones [1], [2], [9]. The BowLeg is a key design element in the ParkourBot design.

To facilitate analysis and control design of running and walking robots, it is convenient to develop simplified models which nonetheless retain the essential character of the original physical system. Examples are the SLIP model of running robots [10]–[12]; the lateral leg spring (LLS) model of the two-legged robots running on a horizontal plane [13], [14]; the ball hopper model [15], which uses a model resembling our SPM model, for primarily horizontal locomotion over rough terrain; the "superball" bouncing ball model [16]; and the "simplest walking model" [17]. Such models can be used to extract important relationships between design and control parameters and performance. For example, Kuo used the simplest walking model to demonstrate that applying an impulse at toe-off is a more energy-efficient way to inject energy into a walker than applying a torque to the stance leg [18].

In this paper, we develop two simplified models of the ParkourBot to analyze the open-loop dynamic stability in the chute-climbing task: the modified SLIP model and the SPM. The SLIP model assumes springy legs of finite stiffness, giving rise to nonzero duration stance phases requiring numerical integration of the equations of motion. The SPM approximates the legs as infinitely stiff, yielding instantaneous stance phases and hybrid dynamics that can be solved analytically.

Our chute-climbing task may be viewed as "vertical running"—the robot locomotes dynamically with alternating foot contacts. Other dynamic multilegged running robots include RHex [19], the Whegs (wheel-legs) robots [20], and Sprawlita [21]. Similar to our robot, these robots use compliant legs that allow them to both scramble over obstacles and locomote relatively efficiently on flat ground.

One aspect of our study that differs from most running robots is that the net motion over many steps is in the vertical direction. While a number of robots have been designed for climbing locomotion, most are quasi-static. The Alicia[3] robot climbs walls by using pneumatic adhesion at one or more of three "cups" connected by two links [22]. The climbing robots in [23] and [24] climb by kinematic or quasi-static bracing between opposing

walls. The four-limbed free-climbing LEMUR robot goes up climbing walls by choosing a sequence of footholds and motions that keep the robot in static equilibrium at all times [25]. Gecko-inspired directional dry adhesives allow Stickybot and Waalbot to climb vertical, smooth surfaces such as glass [26], [27], and the RiSE and SpinybotII robots climb soft or rough walls using spined feet to catch on asperities in the wall [28], [29].

Unlike quasi-static climbers, a few mechanisms [30], [31] have been proposed to achieve a vertical climbing task using dynamic motions while using spines to attach to vertical surfaces. The ParkourBot has no adhesives or clamping mechanisms and cannot maintain height statically. Like runners, the ParkourBot uses dynamics and relies on reaction forces that do not cause slippage, but unlike runners, the ParkourBot's footholds and desired net motion are vertical.

Two model systems that consider "upward" dynamic running, like the SLIP and SPM models of the ParkourBot, are the superball model [16] and the LLS model on inclined planes [32]. The superball model [16] treats the robot as a high-friction ball capable of controlling its angular velocity before impact. A feedback controller is derived for controlled climbing between two vertical walls. To our knowledge, this model system has not been realized experimentally. The LLS model has been used to study the heading stability of two-legged gaits as a virtual insect runs up an inclined plane [32]. This model is similar to the ParkourBot SLIP model in that it alternates touchdown between two spring-loaded legs on either side of the body, and the net motion over several cycles is in the upward direction. It differs in that the impacts can occur anywhere on the inclined plane, while the ParkourBot always impacts two fixed parallel walls. The ParkourBot also has a flight phase, unlike the LLS model. Finally, the ParkourBot body is treated as a point mass due to its gyro-stabilization of body orientation, and the ParkourBot orientation is not open-loop stable without this. The LLS model considers the body orientation as a configuration variable and studies the stability of the insect heading direction.

III. Mechanical Design

The ParkourBot is based on the BowLeg hopper [1]. To adapt it to a climbing scenario, we have decreased the size, provided the robot with two legs, and modified the leg design. We begin by describing the original BowLeg and then discuss the overall design of the ParkourBot including modifications to the BowLegs.

A. BowLeg

The BowLeg [33], a robotic leg concept developed at Carnegie Mellon, integrates the functions and structure of a spring into a lightweight leg. As shown in Fig. 2, the BowLeg resembles an archer's bow, with the hip joint at one end and the foot at the other end of the bow. Made of unidirectional fiberglass (bow glass), the BowLeg can store a large amount of elastic energy, typically enough to lift its own weight 50 m vertically.

When the BowLeg hopper is in flight, an actuator stores energy in the BowLeg by tensioning a string attached to the foot.

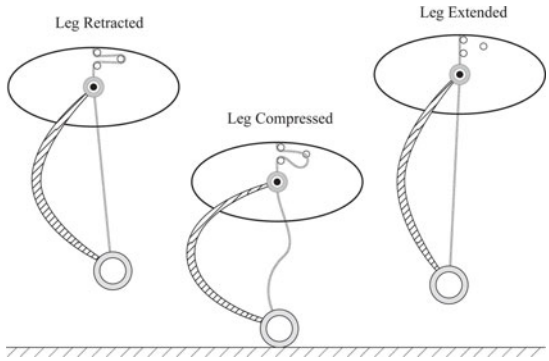

Fig. 2. Schematics of the BowLeg monopod (reprinted from [2] with author's permission).

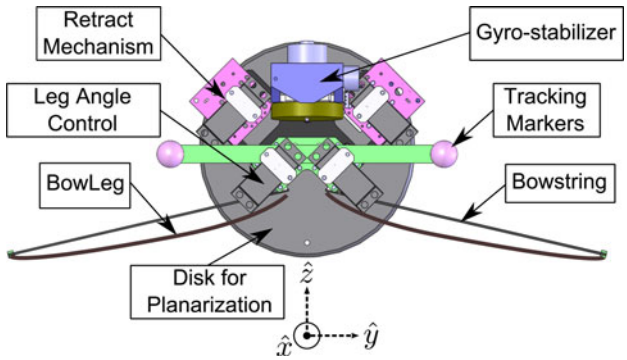

Fig. 3. ParkourBot CAD model.

A separate actuator controls strings to position the leg for the next impact. Upon impact, the strings go slack and the BowLeg quickly releases its stored energy. The leg rotates freely about a hip joint, so that the foot stays in contact with the ground, and no attitude-disturbing torque is transmitted through the joint. Hopping motion is controlled by choosing the angle of the leg at impact and the amount of energy stored in the BowLeg during flight.

B. ParkourBot Design

The main mechanical components of the ParkourBot, depicted in Fig. 3, are the body, the gyro-stabilizer, and two modified BowLegs. The ParkourBot moves in the plane of an air table, where the inertial $\hat{y}$-axis is horizontal, and the $\hat{z}$-axis is "vertical" (opposite the gravity component in the plane of the air table). The $\hat{x}$-axis is normal to the air table.

The body of the ParkourBot consists of a disk that floats freely on the air table, planarizing the system and allowing reduced gravity when the air table is tilted away from vertical. The body carries the microcontroller board, batteries, motor amplifiers, and markers for tracking the motion of the ParkourBot.

The gyro-stabilizer is used to maintain a nearly constant body orientation in the plane of the air table. The gyro-stabilizer consists of a motor spinning a flywheel mounted on a single-axis gimbal attached to the body. The gyro-spin axis is nominally aligned with the world $\hat{z}$-axis. The gimbal permits the gyro to precess about an axis aligned with the $\hat{y}$-axis, stabilizing the attitude about an axis aligned with the $\hat{x}$-axis. A motor and

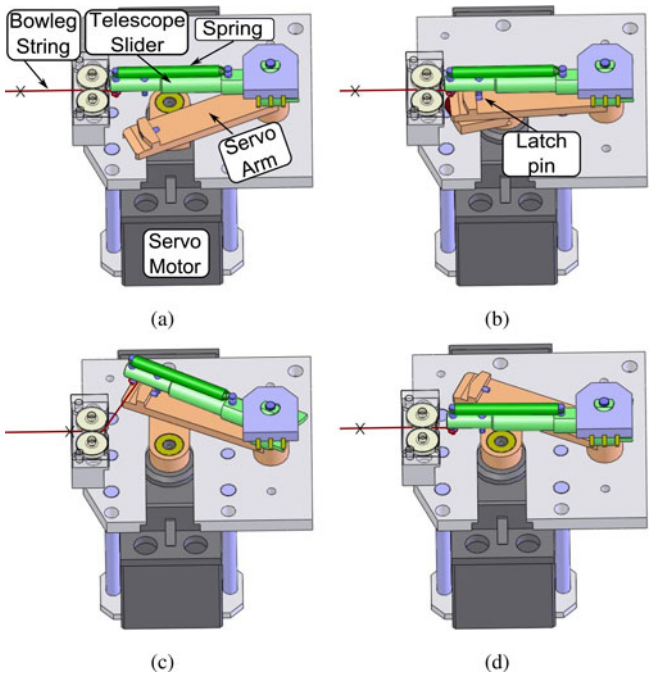

Fig. 4. Retract mechanism sequence. The string is marked with an "x" for length reference. (a) Leg extended, telescope slider fully extended. (b) Servo arm rotates and engages (couples) with a latch pin. (c) Servo arm and the telescope slider rotate together to retract the leg. After wall impact, string goes slack and the spring pulls the telescope slider back. This causes the latch pin to disengage. (d) Telescope slider is pulled back to center by tension in the bowstring. While leg extends and tension builds back in the string, the telescope slider extends and the sequence repeats, with the servo arm now approaching from the other side.

potentiometer attached to the gimbal axis allow active correction of the body orientation.

Each BowLeg consists of a thin unidirectional fiberglass strip that provides the main leg structure and elastic energy storage; a rubber foot pad that enhances foot traction; a hip lever that connects the leg to the hip through a low-friction joint, to minimize the transmitted torque; a bowstring that passes through the hip and connects the foot to the retract mechanism; and a leg-angle control mechanism consisting of a servo at the hip attached to a bar that pulls on two control strings attached to the BowLeg. During stance, these control strings go slack, allowing the leg to rotate freely at the hip. The bowstring retract mechanism pulls on the bowstring and stores potential energy in the BowLeg. It also includes a clutch to release the spring energy when the string goes slack during stance.

The initial design of the retract mechanism for the climber was a miniature version of the BowLeg Hopper's retract mechanism. Reliable release of the string could not be achieved at the smaller scale, however. A new mechanism was conceived and built, as shown in Fig. 4. In the new design, a telescoping slider (green) engages the driven arm (orange) when the string is under tension, allowing the arms to move together, pull the string, and retract the leg. When the string goes slack due to foot contact with the wall, the slider retracts and disengages from the drive arm, releasing the stored energy as the foot kicks off the wall.

TABLE I
PARAMETERS USED IN ANALYSIS OF THE PARKOURBOT

Description	Symbol	Dimensional	nondimensional
body mass	m	1.548 kg	1
leg rest length	ℓ	0.193 m	1
gravity	g	1.478 m/s^2	1
wall width	d	0.54 m	2.798
SLIP Model			
leg spring stiffness	k	525 N/m	44.286
leg linear damping	c_ζ	1 Ns/m	0.3614
leg rotational damping	c_ψ	1 Ns	0.2853
SPM			
restitution coefficient	ϵ		0.7

IV. MODELING

In this section, we derive two different models of the ParkourBot's motion in a chute: the SLIP model and the SPM. The SLIP model assumes a springy leg of finite stiffness, giving rise to a nonzero duration stance phase requiring numerical integration of the equations of motion. The SPM approximates the leg as infinitely stiff, giving rise to equations of motion that can be solved analytically. For each of these models, we study fixed points and the stability of the open-loop climbing dynamics.

In our nondimensional modeling, the characteristic mass is the mass m of the ParkourBot, the characteristic length is the length ℓ of an unretracted BowLeg, and the characteristic time is $\sqrt{\ell/g}$, where g is the gravitational acceleration in the $-\hat{z}$ direction. In the rest of this section, all nondimensional analysis is based on the properties of the experimental system. In particular, our ParkourBot mass is approximately $m = 1.548$ kg, the rest leg length is $\ell = 0.193$ m, and gravity on the inclined air table is $g = 1.478$ m/s^2. The nondimensional distance between the two vertical walls is $d = 2.798$, which is based on the dimensional distance of 0.54 m. The relevant parameters are summarized in Table I, including parameters used in the SLIP model and the SPM. The BowLeg stiffness was estimated using a spring scale, and the damping parameters were chosen to fit simulations to the experimental trajectories. By an abuse of notation, we use the same symbol to refer to both the dimensional and nondimensional values of the parameter; throughout the rest of this section, all usages refer to the nondimensional value.

A. Simplifications

We exploit the symmetry in the ParkourBot's design and environment by assuming that stance always occurs on the right wall. A single stride of the ParkourBot consists of free flight from the right wall to the left wall, a coordinate flip upon reaching the left wall so that the ParkourBot is instantaneously moved to the right wall with a reversed horizontal velocity, and a stance phase on the right wall. By exploiting this symmetry, we can use the same set of coordinates for each stance phase.

Our simplified models of the ParkourBot are based on the following considerations.

1) The BowLegs have much less mass than the body. Therefore, we treat the BowLegs as massless.
2) The feet have a high friction coefficient with the wall, approximately $\mu = 2$, so we assume no slip during stance.

(This assumption is occasionally violated during experiments, usually leading to falls.)

3) The hip joint supports very little torque, meaning that contact forces during stance are along the line from the foot to the hip. This line passes approximately through the body center of mass so that the stance phase generates very little attitude-disturbing torque on the body. This fact, coupled with the attitude-stabilizing effect of the gyrostabilizer, allows us to remove body orientation from the description of the configuration.

With these considerations, the nondimensional configuration of the ParkourBot is simply (y, z), the location of the point-mass body, and its nondimensional velocity is $(\dot{y}, \dot{z})$. The control inputs are $\psi_0 > 0$, the angle of the leg below horizontal at the beginning of the stance phase, and $\sigma \geq 0$, the nondimensional energy stored in the leg that is released during the stance phase. When the leg stores nonzero energy just before touchdown, its nondimensional retracted length is $\zeta_0 < 1$. If the leg is modeled as a linear spring, then $\sigma = \frac{1}{2}k(1-\zeta_0)^2$, where k is the nondimensional spring stiffness. Thus, we can represent the energy input control as either σ or ζ_0 for a linear spring. (For an infinitely stiff spring, $\zeta_0 = 1$ for any stored energy σ.)

In this paper, we focus on open-loop climbing. Therefore, for the rest of the paper, we consider only the case of constant inputs, $\zeta_0(k) = \zeta_0$ and $\sigma(k) = \sigma$, and study the fixed points of the dynamics, their bifurcations, and stability.

B. Poincaré Map of the Complete Dynamics

As mentioned previously, a single stride of the ParkourBot from one wall to another consists of three steps: 1) free flight from the right wall to the left wall; 2) upon reaching the left wall, a coordinate transformation to reverse the horizontal velocity and place the ParkourBot on the right wall; and 3) a stance phase on the right wall. It will be convenient to define the beginning of a stride at step 2, and write the dynamics of a full stride as the coordinate flip, followed by stance, followed by free flight to the left wall. The inertial frame xyz is centered between the two walls (see Fig. 5).

Let $\bar{x} = [y, z, \dot{y}, \dot{z}]^T$ be the full state of the ParkourBot and $\bar{x}(k)$ be the state of the ParkourBot just before reaching the left wall (before the coordinate flip) for the kth time. Then, for a given set of controls, we can express an entire stride as

$$\bar{x}(k+1) = \bar{P}(\bar{x}(k)) = \bar{f}_{\text{flight}}(\bar{f}_{\text{stance}}(\bar{f}_{\text{flip}}(\bar{x}(k)))) \quad (1)$$

where $\bar{f}_{\text{flip}}$, $\bar{f}_{\text{stance}}$, and $\bar{f}_{\text{flight}}$ represent the coordinate flip, stance, and flight, respectively. The coordinate flip is simply

$$\bar{f}_{\text{flip}}(\bar{x}) = [-y, z, -\dot{y}, \dot{z}]^T.$$

The free-flight dynamics can be expressed as

$$\bar{f}_{\text{flight}}(\bar{x}) = \begin{bmatrix} y + T\dot{y} \\ z + T\dot{z} - \frac{1}{2}T^2 \\ \dot{y} \\ \dot{z} - T \end{bmatrix}$$

where T is the nondimensional flight time. To calculate the flight time T, note that the ParkourBot body must travel a distance

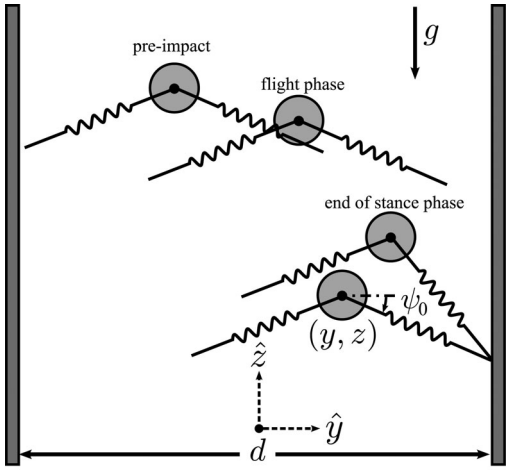

Fig. 5. Notation for the ParkourBot models. The resting leg length is $\zeta_0 = 1$, the retracted leg length just before impact is $\zeta_0 \leq 1$, (y, z) is the location of the point mass body, and ψ_0 (which is positive as shown) is the angle of the leg with respect to the horizontal just before impact.

$r < 0$ to reach the left wall, where

$$r = -y - \frac{d}{2} + \zeta_0 \cos\psi_0$$

ψ_0 is the BowLeg angle control, and ζ_0 is the leg length corresponding to the stored energy control σ. (Note that these controls are for the *next* impact, i.e., $\psi_0(k+1)$ and $\sigma(k+1)$.) The flight time is simply

$$T = \frac{r}{\dot{y}}.$$

To solve for the complete stride map $\bar{P}$, all that is needed is the stance phase dynamics f_{stance}. We introduce two possible models for the stance phase dynamics: the SLIP model (see Section IV-C) and the SPM (see Section IV-D).

Before doing so, however, note that we can eliminate the variable $y(k)$ from the description of $\bar{x}(k)$, since it is uniquely determined by the BowLeg angle control $\psi_0(k)$ and the preimpact leg length $\zeta_0(k)$

$$y(k) = -\frac{d}{2} + \zeta_0(k)\cos\psi_0(k). \quad (2)$$

Thus, we define a Poincaré section at the state where the ParkourBot reaches the left wall, as defined by (2). We use this section to reduce the state vector by one variable.

Finally, we often eliminate $z(k)$ from the state description, as we can analyze the stability of the stride map independent of the robot's height. The new state vector is $x(k) = [\dot{y}(k), \dot{z}(k)]^T$, and our stride Poincaré map is

$$x(k+1) = P(x(k)) = f_{\text{flight}}(f_{\text{stance}}(f_{\text{flip}}(x(k)))) \quad (3)$$

where f_{flight}, f_{stance}, and f_{flip} are the same as the mappings above, but without the first two rows.

C. Spring-Loaded Inverted Pendulum Model

1) Spring-Loaded Inverted Pendulum Model Details: In this section, we derive the stance phase dynamics using the

SLIP model to solve the complete map P' introduced in Section IV-B. During stance phase, it is convenient to replace the cartesian coordinates with polar coordinates and represent the configuration as $(\zeta(t), \psi(t))$, where $\zeta(t)$ is the leg length, $\psi(t)$ is the leg angle, and nondimensional time t runs from 0 (at leg touchdown) to the time of liftoff. Since the leg is massless, touchdown occurs without impact with $\zeta(0) = \zeta_0$ and $\psi(0) = \psi_0$. Liftoff occurs when the ground reaction force on the leg vanishes, i.e., when $k - k\zeta - c_\zeta \dot{\zeta} = 0$.

The nondimensional Lagrangian in polar coordinates during stance phase is

$$L = \frac{1}{2}(\dot{\zeta}^2 + \zeta^2 \dot{\psi}^2) - \frac{k}{2}(1-\zeta)^2 - \zeta \sin\psi. \tag{4}$$

To better capture the physical system, we add linear and rotational damping terms to the stance phase equations of motion, c_ζ and c_ψ, acting along the leg and at the pivot with the wall. After adding these viscous damping terms, we arrive at a set of nondimensional equations of motion of f_{stance} of the SLIP model

$$\begin{aligned} \ddot{\zeta} &= k - k\zeta + \zeta\dot{\psi}^2 - \sin\psi - c_\zeta \dot{\zeta} \\ \ddot{\psi} &= -\frac{1}{\zeta}(\cos(\psi) - 2\dot{\zeta}\dot{\psi}) - c_\psi \dot{\psi}. \end{aligned} \tag{5}$$

Using these equations of motion, the full stride map in (1), as well as the Poincaré map in (3), can be evaluated. Despite the simplicity of the model, there is no closed-form solution of the stance phase. Thus, analysis and simulation in the next section are done numerically.

2) Analysis of the Spring-Loaded Inverted Pendulum Model: In this section, we carry out a numerical investigation of the SLIP model based on parameters corresponding to our actual ParkourBot setup. The nondimensional BowLeg spring coefficient, $k = 44.286$, was estimated by measuring the displacement of the leg to a known load. The nondimensional damping coefficients, $c_\zeta = 0.3614$ and $c_\psi = 0.2853$, were approximated from experimental drop test data.

a) Fixed points and local stability: A period-n fixed point is a point on the Poincaré section that is mapped back to itself after applying the Poincaré map P n-times. A period-n fixed point for a constant set of controls is called a *gait*. To determine the local stability of a gait, we calculate the Jacobian of the map P^n with respect to x and examine its eigenvalues. If both eigenvalues lie within the unit circle, the fixed point is stable.

b) Bifurcations: For a range of constant control inputs, we found a single stable period-1 gait. Small changes in the controls (or another parameter) can cause a new stable period-2 gait to emerge from the (now unstable) period-1 solution at a bifurcation point. Fig. 6 depicts the case for varying the leg angle control ψ_0 while keeping ζ_0 and other parameters fixed. The plots of one of the two variables on the Poincaré section $\dot{y}$ show period doubling as ψ_0 increases. For larger energy input (smaller ζ_0), the onset of period doubling occurs at lower values of ψ_0. These plots are created by simulating the ParkourBot until convergence, then plotting the next 50 points. The plots are truncated at large values of ψ_0 as the simulated model of the ParkourBot "trips"; the post-impact velocity of the ParkourBot is not away from the impact wall, but continuing toward the wall. The ParkourBot crashes into the wall and the simulation is terminated.

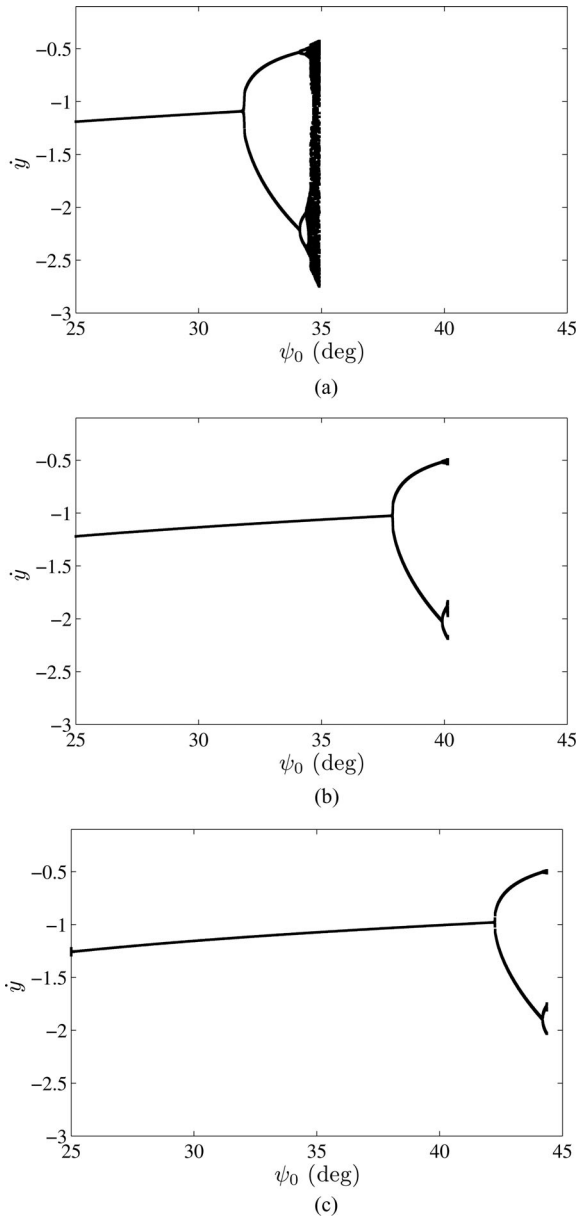

Fig. 6. Bifurcation plot of $\dot{y}$ (nondimensional) while changing the leg angle control for three different leg energy inputs. The plots show period doubling bifurcation as ψ_0 increases. For larger energy input (smaller ζ_0), the onset of period doubling occurs at lower values of ψ_0. (a) Leg retraction: $\zeta_0 = 0.65$. (b) Leg retraction: $\zeta_0 = 0.75$. (c) Leg retraction: $\zeta_0 = 0.85$.

These bifurcation plots indicate the existence of stable period-1 gaits with constant (open-loop) controls. In experiment, however, we cannot obtain perfectly constant controls, due to asymmetries in the physical design of the ParkourBot. In particular, when we command a leg angle ψ_0, we get a slightly different angle for the left leg than we get for the right leg. In addition, the energy storage bowstrings are activated by pulling "up" or "down" on the string [see Fig. 4(c)] on alternating strides, yielding slightly different leg retracts. This can result in effectively

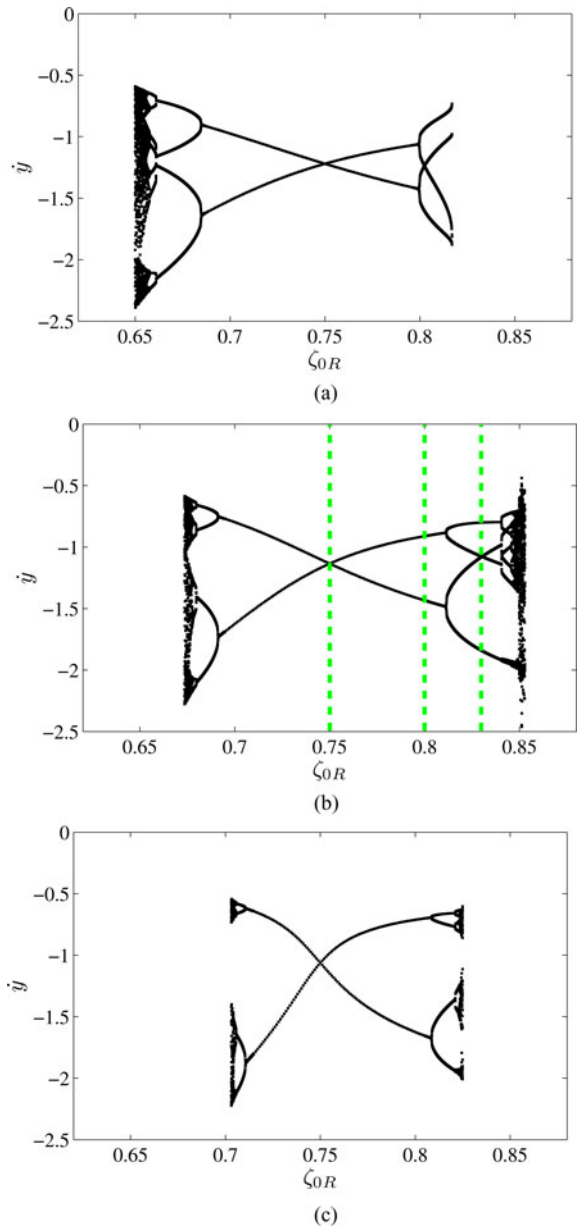

Fig. 7. Bifurcation plot of $\dot{y}$ (nondimensional) for three different leg angles while changing the leg energy input (nondimensional leg retraction) of the right leg. Left leg retraction remains constant ($\zeta_{0L} = 0.75$). Vertical lines in (b) correspond to Period-1, Period-2, and Period-4 portrayed in Fig. 8. (a) Leg angle: $\psi_0 = 25^\circ$. (b) Leg angle: $\psi_0 = 30^\circ$. (c) Leg angle: $\psi_0 = 35^\circ$.

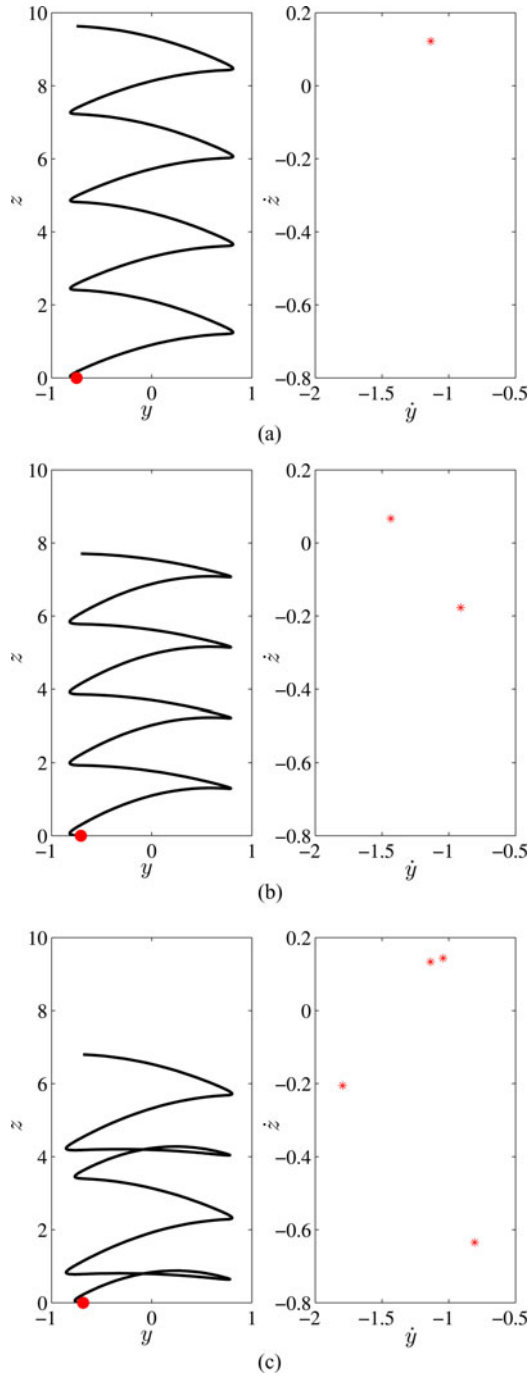

Fig. 8. Nondimensional trajectories and fixed points of stable gaits corresponding to vertical dashed lines in Fig. 7(b). Left column shows the trajectory of eight consecutive leaps starting from a fixed point (solid circle), and right column shows the fixed points on the Poincaré section (red "*"). Leg angle $\psi_0 = 30^\circ$ and left energy input $\zeta_{0L} = 0.75$ in all three gaits. Controls: (a) $\zeta_{0R} = 0.75$. (b) $\zeta_{0R} = 0.8$. (c) $\zeta_{0R} = 0.825$. All figures are nondimensional. (a) Stable period-1 climbing with $\psi_0 = 30^\circ$ and $\zeta_{0L} = \zeta_{0R} = 0.75$. (b) Stable period-2 climbing with $\psi_0 = 30^\circ, \zeta_{0L} = 0.75, \zeta_{0R} = 0.8$. (c) Stable period-4 climbing with $\psi_0 = 30^\circ, \zeta_{0L} = 0.75, \zeta_{0R} = 0.825$.

four different controls when constant controls are commanded: the left leg angle with bowstring up and down, and the right leg angle with bowstring up and down. Thus, a nominal period-1 gait can look more like a period-4 gait in experiment.

In Fig. 7, we conduct a numerical study of the case where the right and left leg angles are identical but the stored energy in each leg is slightly different. In each of Fig. 7(a)–(c), the left leg retract ζ_{0L} is held constant at 0.75, while ζ_{0R} is varied. In all three plots, the stable gait is period-1 when the retracts are identical, but period doubling is observed as ζ_{0R} changes. Similar bifurcations appear in other walking [34], [35] and climbing systems [3]. Looking at the bifurcation plot with leg angle $\psi_0 = 30^\circ$ [see Fig. 7(b)], we mark three values of ζ_{0R} with a vertical dashed line. The three dashed lines correspond to period-1, period-2, and period-4 gaits, for which we show the trajectories and Poincaré sections in Fig. 8.

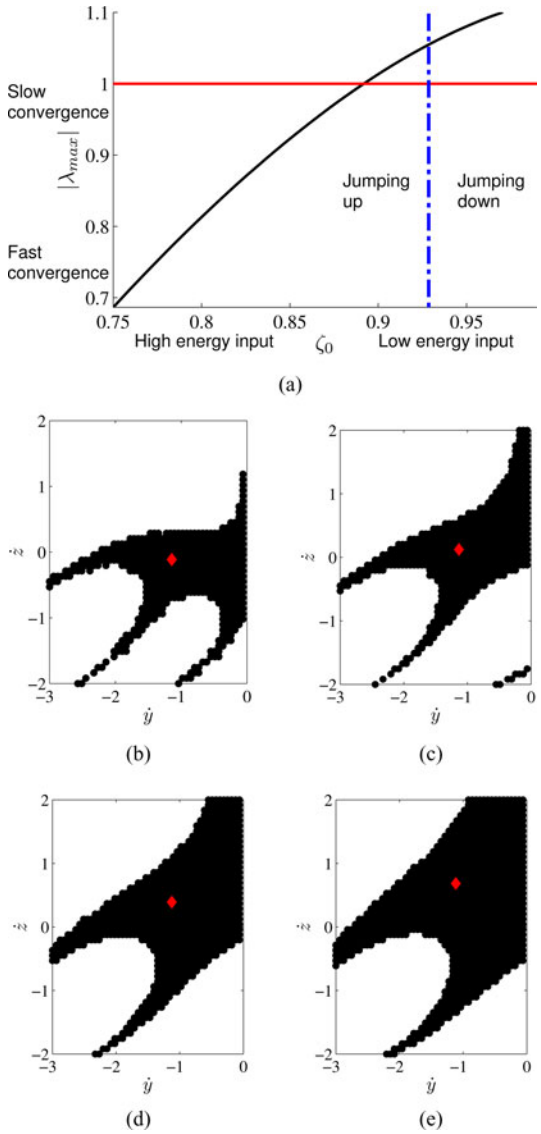

Fig. 9. Varying energy input (ζ_0) for a constant leg angle $\psi_0 = 30°$ for the SLIP model. All fixed points are period-1 motions (marked as red stars). (a) The maximum eigenvalue magnitude of the Jacobian for the fixed point as a function of ζ_0. Blue dashed line indicates critical ζ_0 for jumping in place; energy input to the right of blue dashed line corresponds to climbing down. (b)–(e) Basins of attraction to the fixed point (in red) on the Poincaré section $(\dot{y}, \dot{z})$ for various energy levels. As the energy input increases the local stability increases (lower eigenvalues) and the area of the BOA increases. The normalized areas of BOAs are approximately 0.490, 0.563, 0.813, and 1, respectively. All figures are nondimensional. (a) Maximum eigenvalue versus energy input. (b) $\zeta_0 = 0.8$. (c) $\zeta_0 = 0.75$. (d) $\zeta_0 = 0.7$. (e) $\zeta_0 = 0.65$.

c) Varying energy input: Fig. 9 shows a correlation between energy input (the amount of leg retraction) and the stability of the system for $\psi_0 = 30°$. For all leg retracts considered, the only stable gaits are period-1. The figure shows that higher input energy (lower ζ_0) corresponds to faster convergence to the period-1 gait and a larger basin of attraction (BOA), which is the set of all initial velocities that converge to the period-1 gait. (Points outside the BOAs generally lead to a "trip," where the post-impact velocity of the ParkourBot is still toward the impact wall.) Roughly, the system is more stable with large energy inputs, which results in high-speed upward climbing. The figure also shows that the period-1 gait becomes unstable when the energy input is too low, and the ParkourBot is not capable of stable climbing down for the chosen parameters and leg angle.

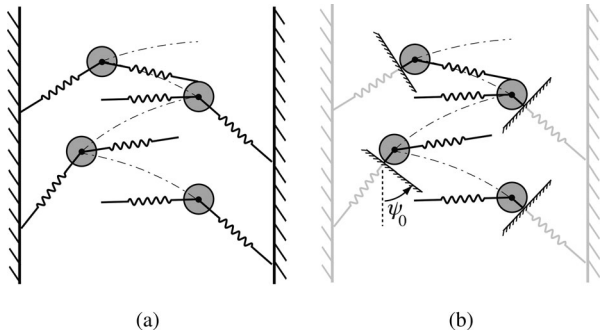

Fig. 10. "SPM." (a) Cartoon of a typical climb, equivalent to (b) a stiff ball bouncing on surfaces sloped from the vertical at angles equivalent to the leg angles ψ_0.

D. Simplest Parkour Model

1) Simplest Parkour Model Details: In this section, we derive the stance phase dynamics using the SPM to solve the complete Poincaré map P' introduced in Section IV-B. The springy legs are modeled as infinitely stiff with $\zeta_0 = 1$, leading to an instantaneous stance phase. Similar to the analysis in [2] and [9], this model is similar to a stiff ball bouncing on a surface whose slope can be controlled at each impact, as illustrated in Fig. 10. Impacts occur at $y = \pm a$, where $a = d/2 - \cos\psi_0$. At impact, the kinetic energy KE is governed by

$$(KE)^+ = \epsilon(KE)^- + \sigma \tag{6}$$

where $\epsilon \in [0, 1]$ is a restitution coefficient representing energy loss, σ is energy injected at impact, and the superscripts $-$ and $+$ refer to just before and after impact. Positive σ corresponds to converting the energy stored during the flight phase into kinetic energy, whereas negative σ corresponds to storing more energy in the spring at impact. The ParkourBot is not capable of negative σ, but future designs may be based on this idea.

At impact, an impulse is applied along the leg through the mass. We represent the robot's velocity at impact as

$$\begin{bmatrix} v_n \\ v_r \end{bmatrix} = \begin{bmatrix} \sin\psi_0 & \cos\psi_0 \\ -\cos\psi_0 & \sin\psi_0 \end{bmatrix} \begin{bmatrix} \dot{y} \\ \dot{z} \end{bmatrix}$$

where (v_n, v_r) represent the normal (perpendicular to the impact leg) and radial (along the leg toward the mass) velocities, respectively. Since the impulse can only influence the radial velocity, the normal velocity remains constant through the impact. The impact map representing the stance phase of the SPM is

$$y^+ = y^-,\ z^+ = z^-,\ v_n^+ = v_n^-,\ v_r^+ = \sqrt{\epsilon(v_r^-)^2 + 2\sigma}. \tag{7}$$

Using this impact map, the full Poincaré map as in (3) can be expressed in a closed form.

2) Analysis of the Simplest Parkour Model: It can be shown that the period-1 fixed points of the Poincaré map in (3) for the

SPM can be written in a closed form as

$$\dot{y}_* = -\sqrt{a\cot\psi_0}, \quad \text{and} \tag{8}$$

$$\dot{z}_* = \sqrt{a\cot\psi_0}\,(-\tan\psi_0 + C) \tag{9}$$

where

$$C = -\frac{2}{(1-\epsilon)\sin 2\psi_0}\left(1+\epsilon-\sqrt{4\epsilon+(1-\epsilon)\frac{\sigma}{a}\sin 2\psi_0}\right).$$

This corresponds to a nondimensional change in height h at each stride of

$$h = 2aC. \tag{10}$$

Given a desired stride height h, we can solve (10) for the injected energy control σ as

$$\sigma = a\left(\frac{(1-\epsilon)}{\sin 2\psi_0} + \frac{(1+\epsilon)h}{2a} + \frac{(1-\epsilon)h^2\sin 2\psi}{16a^2}\right) \tag{11}$$

which allows us to reparameterize the fixed point with h as

$$\dot{y}_* = \sqrt{a\cot\psi_0}, \quad \text{and} \tag{12}$$

$$\dot{z}_* = \sqrt{a\cot\psi_0}\left(-\tan\psi_0 + \frac{h}{2a}\right). \tag{13}$$

With this parameterization, we may be able to create motion plans more easily in real time than with the numerical results of the SLIP model.

For the analysis of the SPM in this section $d = 2.798$ and $\epsilon = 0.7$. The restitution coefficient was empirically approximated as described in Section V-B. Using these parameters and a leg angle of $\psi_0 = 30°$, we computed the fixed points and the maximum eigenvalues of their Jacobians over a range of input energies as shown in Fig. 11(a), which shows climbing up is more stable than descending. Fig. 11(b)–(e) show the BOA for energy controls $\sigma = 0, 0.025, 0.05$, and 0.075, and fixed leg angle $\psi_0 = 30°$. The area of the BOA for the SPM decreases with decreasing energy levels, similar to that of the BOA for the SLIP model.

The SLIP model and the SPM demonstrate similar qualitative behavior in the BOA and local stability approximations. The main exception is that we have observed no period-n gaits for $n > 1$ for the SPM. The SPM naturally gives rise to higher period solutions when incorporating asymmetric controls due to the slight asymmetry of the ParkourBot design, as described in Section IV-C2b. Another exception is that the SPM predicts the existence of open-loop stable downward climbing, while the SLIP model does not, when the models are populated with our best estimates of the parameters of the experimental ParkourBot. We come back to this in the discussion of the experiments in Section V-C.

To understand how energy and leg actuator force requirements scale with gravity and the distance between the chute walls, we use (11) for the amount of energy injected for a desired hopping height. Converting (11) back to a dimensional equation and setting h to zero to maintain hopping height, the equation becomes $\sigma = \frac{mga(1-\epsilon)}{\sin 2\psi_0}$. Therefore, in order to maintain the steady-state hopping height the robot must store energy in the leg, which grows linearly with gravity, mass of the robot, and the distance between the walls for a fixed leg angle. Since energy in a spring is $(1/2)kx^2$, and force f is kx, then energy in the spring is $f^2/2k = \sigma$. Therefore, the force in the spring is $\sqrt{2k\sigma}$, and if either gravity g or the distance between the walls a increases by a factor r, the force required to retract the spring grows by $\sqrt{r}$.

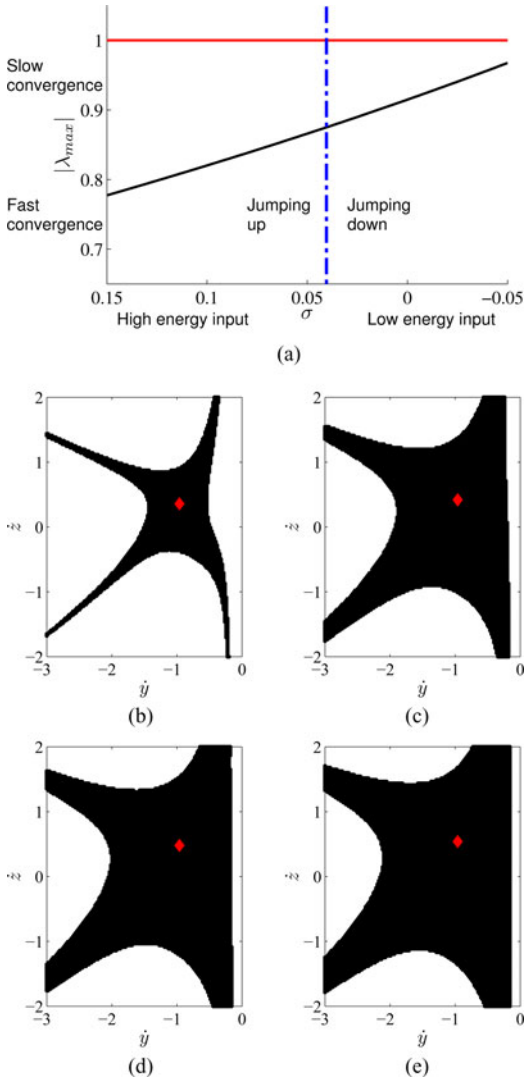

Fig. 11. Stability versus energy input with a leg angle $\psi_0 = 30°$ for the SPM model. (a) Maximum eigenvalue magnitude as a function of the injected energy (σ). To the left of the blue-dashed vertical line climbing is upward. Climbing up is more stable than descending. (b)–(e) BOA on the Poincaré section ($\dot{y}, \dot{z}$) for four energy inputs. Red stars mark the period-1 attractor. Similar to Fig. 9, as the energy input increases, so does the area of the BOA. All figures are nondimensional. (a) Maximum eigenvalue versus energy input. (b) $\sigma = 0$. (c) $\sigma = 0.025$. (d) $\sigma = 0.05$. (e) $\sigma = 0.075$.

V. Experiments

A. Experimental Setups

We use a tilted air table (see Fig. 12) for the test environment, which enforces the planar constraint and provides an easy way to change the effective gravity by tilting the table. Since the contact between the ParkourBot and the table is frictionless, this setup is equivalent to pure vertical climbing in a reduced gravity environment. The Coulomb friction coefficient between

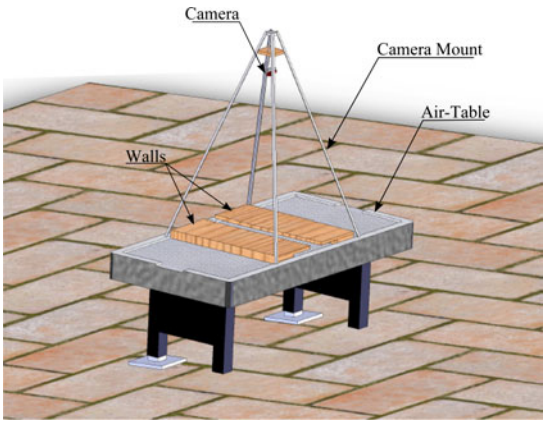

Fig. 12. Experimental setup consists of a vision-tracking system and a tilted air table enforcing planarity and providing a lower effective gravity.

the rubber foot and wall was observed to be about $\mu = 2.0$, thus making foot slipping rare. For the model validation of the SPM (see Section V-B), we use a high-speed *PhotonFocus* $^{\text{tm}}$TrackCam at 1000 Hz to measure ParkourBot trajectories. To track the ParkourBot during the open-loop climbing experiments (see Section V-C), we use a Natural Point$^{\text{tm}}$FLEX V100 IR camera mounted above the air table at a framerate of 100 Hz. The camera provides positions of all IR reflectors to a PC, which communicates with the robot over wireless XBee protocol. Mechanism and environment parameters are identical to the ones used in the analysis and given in Table I. The leg angles for the following experiments were obtained using $\psi_0 = 30°$.

B. Simplest Parkour Model Validation

We recorded the trajectory through impact for many impacts with various leg retract controls and fixed leg angles of $\psi_0 = 30°$. The leg retract controls correspond to different injected energies σ.

A recording for a single jump cycle is shown in Fig. 13(a). As shown in Fig. 13(b), the body angle stays approximately constant throughout the trajectory due to the gyro-stabilizer, allowing us to ignore orientation in the SPM. During flight, the horizontal and vertical positions, respectively, follow linear and quadratic trajectories as predicted by ballistic motion, shown in Fig. 13(c) and (d). We fit linear and quadratic regressions to the pre- and postflight positions. The impact is estimated to occur at the intersection of the linear regressions. With this method, we do not estimate the robot's state during the stance phase and focus on finding an instantaneous impact state that is compatible with the two flight phases. With the regressions, we estimate the pre- and post-impact states for the SPM. To compute the normal and radial velocities, we calculate the effective angle ψ with the wall by combining the angles of the leg and the body.

The kinetic energy and normal velocity for post- versus pre-impact for three sample energy controls (energy C>energy B>energy A) over many impacts can be seen in Fig. 14(a) and (b), respectively. The different energy levels correspond to different servo retraction values. The slopes of linear regressions of the energy data were averaged over many controls to produce

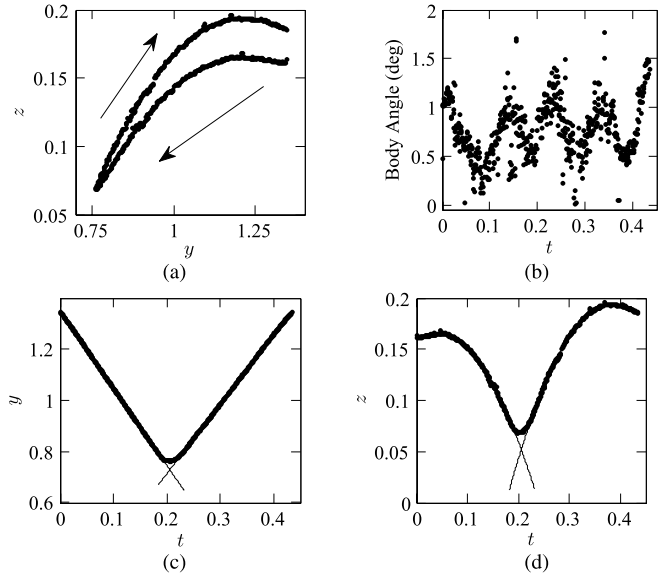

Fig. 13. (a) Recorded (y, z) trajectory of ParkourBot for one jump cycle. (b)–(d) Body angle nondimensional horizontal position y, and nondimensional vertical position z as a function of nondimensional time, respectively, of the ParkourBot for one impact. (c) and (d) have linear and quadratic regressions overlaid for preimpact and postimpact flights. All figures are nondimensional.

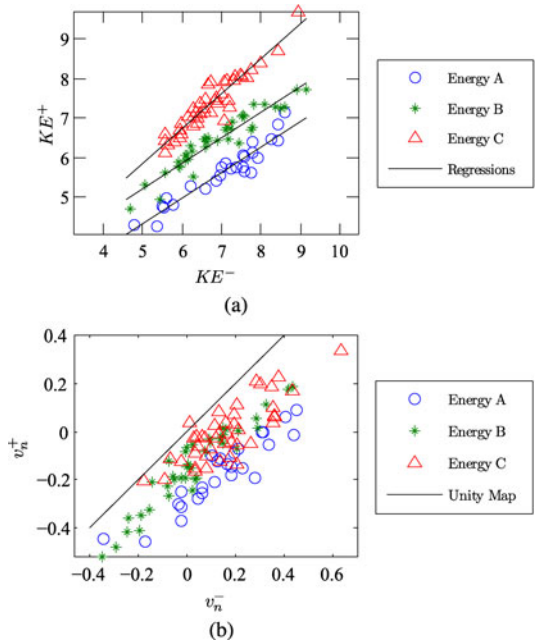

Fig. 14. (a) Post- versus pre-impact nondimensional kinetic energy with linear regressions. (b) Post- versus pre-impact normal velocity with ideal map ($v_n^+ = v_n^-$). As can be seen, experimental data are mostly below the unity map, which is expected due to the loss of kinetic energy associated with the normal velocity.

$\epsilon = 0.7$, which is comparable to energy loss measured with the single-leg BowLeg hopper [2]. The energy intercept gives an approximately linear relationship between the leg retract control and the injected energy. These experiments show that the SPM can be used to approximately model the ParkourBot.

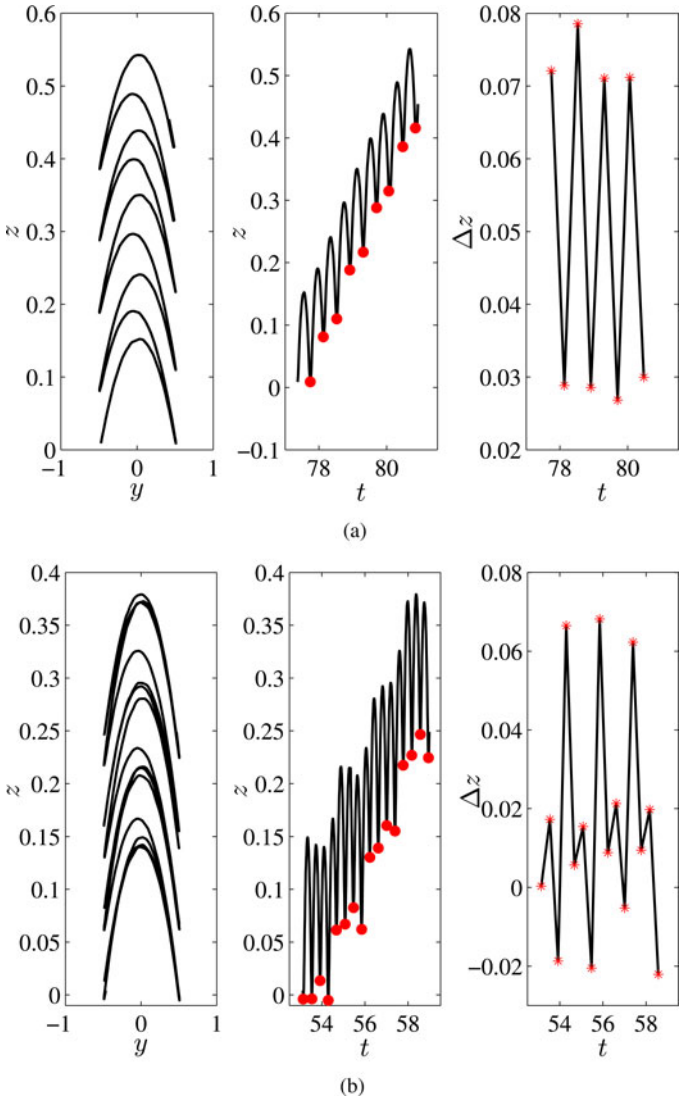

Fig. 15. Experimental data of open-loop climbing. Climbing trajectory (left column), height z versus time (middle column), where the circles indicate the Poincaré section, and Δz between pairs of consecutive states on Poincaré section (right column). (a) Stable period-2 climbing up. (b) Stable period-4 climbing up. All figures are nondimensional. (a) Period-2. (b) Period-4.

C. Open-Loop Climbing Results

Motivated by the existence of stable period-n open-loop gaits, the goal of our open-loop experiments was to validate the existence of these gaits experimentally. We readily observed what appeared to be period-2 and period-4 gaits, but did not observe period-1 motions, perhaps due to the mechanical asymmetries discussed in Section IV-C2b. Fig. 15 shows sample period-2 and period-4 experimental results. (See supplementary attachment for a video of this experiment.) To get a sense of stability, we use Mean Jumps To Failure (MJTF), similar to [36]. We chose ten different energy levels and ran eight experiments for each energy level. For each individual experiment, we counted the number of jumps before crash, as seen in Fig. 16. This plot correlates to our simulation results in Fig. 9, showing how the system is more stable when the input energy is increased. The most stable climbing occurs at high-energy input (fast climbing) on the left side of Fig. 16, but the robot crashes when it reaches the top of the chute, explaining why the MJTF begins to drop at high-energy input. For low-energy input on the right side of Fig. 16, the robot descends slowly, apparently indicating that open-loop downward climbing is possible, as predicted by the SPM model but not the SLIP model. It is difficult to know for certain whether descending is truly stable, however, as the number of successful jumps, before the robot trips and falls, decreases.

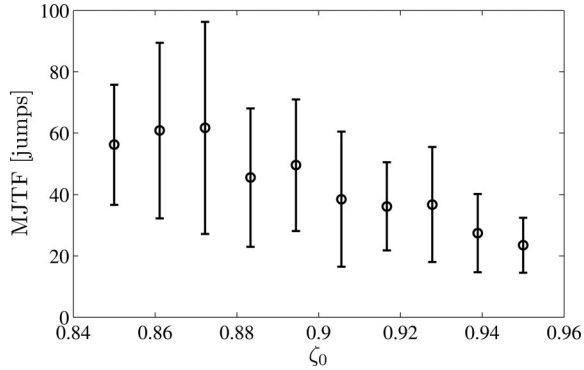

Fig. 16. MJTF versus nondimensional leg retraction ζ_0. The vertical axis shows the average number of jumps before crash, with error bars representing the standard deviation. Leg retraction ζ_0 was roughly approximated. Eight experiments were conducted for each energy level.

VI. Discussion

There is qualitative agreement between the SLIP model and SPM's predictions of local stability and BOA, with the caveat that the SPM does not predict period-n gaits for $n > 1$ under the assumption of fixed symmetric controls. The SLIP model converges to the SPM as the stiffness of the leg is increased, but away from this limit it is difficult to make quantitative comparison between the two models due to the different parameters in the stance phase. Moreover, it is difficult to distinguish whether the source of higher period gaits in the experimental platform is due to slight asymmetries in the robot design or a fundamental property of the dynamics, as predicted by the SLIP model but not the SPM. The closed-form SPM may be particularly useful for real-time motion planning, a direction of future work.

There are a few limitations of the current ParkourBot mechanism and experimental arena.

1) The ParkourBot is currently launched manually. The launch must have little initial angular momentum in order to satisfy the assumption of zero change in orientation. Good launches can be achieved with a little practice, but it is difficult to achieve nearly identical initial conditions.
2) Slight asymmetries in the mechanical design mean that identical commanded controls do not necessarily lead to identical leg angles and injected energy (see Section IV-C2b).
3) The gyro-stabilizer gimbal has a limited angle range. When a limit is reached, the gyro-stabilizer can no longer correct body orientation drift in one direction.
4) The line of action of the springy leg is approximately through the center of mass of the body, resulting in little

attitude-disturbing torque when the robot is in stance. The disturbance torque grows as the leg angle moves away from approximately $\psi = 30^\circ$, however. In practice, this means that the usable leg angle control range is small.

5) The limited torque of the leg retract servos limits the amount of energy that can be stored in the BowLegs. This limits the current ParkourBot to climb in gravity of approximately 2 m/s^2 or less. Using the approximated energetics described at the end of Section IV-D, for the current mechanism to be able to maintain height in full gravity the actuator must be approximately 2.2 times stronger.
6) The limited height of the chute prevents long climbs. We could potentially replace the side walls with conveyor belts to allow longer virtual climbs.

The usual failure mode of the robot is drift in body orientation leading to a fall. This can be mitigated by the use of feedback control of the gyro-stabilizer, up to the gimbal limits. Feedback control on the robot height can further be used to reliably stabilize hopping for 100 touchdowns or more [37]. An alternate approach to orientation control, not used in the current ParkourBot, involves the use of a reaction wheel rotating about the $\hat{x}$-axis, not the $\hat{z}$-axis as for the gyro-stabilizer. Moreover, applying a torque during stance phase similar to Raibert's hoppers [7], [8] could not be applied due to the BowLeg's loss of control authority during stance phase.

The ParkourBot prototypes use a 6-V 2.3-Ah battery pack to power the gyro-stabilizer, leg retract servo, leg angle servo, and microcontroller for approximately 30 min between charges. We have run numerous experiments over the past two years totaling over 6 h of climbing time and over 60 000 leaps with only a few replacements of the leg retract and angle control strings.

VII. Conclusion and Future Work

This paper demonstrates the first use of dynamic leaping by a two-legged robot to climb up a vertical channel in reduced gravity. The ParkourBot uses low-power actuators to store elastic energy in the springy legs during flight phases, and this energy is released in high-power events during the brief stance phases. We have derived two simplified models of the system, the SLIP model and the SPM, which capture the essential dynamics of the ParkourBot and predict stable open-loop climbing gaits. These stable open-loop climbing gaits have been demonstrated in experiments on the ParkourBot.

Future directions for the parkour project include: 1) feedback control of climbing using high-speed vision (early work in this direction is described in [37]); 2) vertical climbing in full Earth gravity; 3) motion planning and control in more complex planar environments, with footholds at a variety of positions and orientations, along with tools to estimate the set of reachable states in such environments; and 4) eventually full 3-D parkour, with dynamic maneuvers beyond leaping, where each handhold or foothold the environment offers can be viewed as a potential source of reaction forces.

Acknowledgment

The authors would like to thank G. Zeglin for the use of his explanations of the BowLeg concept, N. Rosa for assistance with the TrackCam, and T. Phillip and N. Rosa for numerous discussions. They would also like to thank K. Goldberg for early discussions on the possibility of the ParkourBot.

References

[1] H. B. Brown and Jr, G. Zeglin, "The Bow Leg hopping robot," in *Proc. IEEE Int. Conf. Robot. Autom.*, May 1998, pp. 781–786.
[2] G. Zeglin, "The Bow Leg hopping robot," Ph.D. dissertation, Robotics Institute, Carnegie Mellon University, Pittsburgh, PA, USA, Oct. 1999.
[3] A. Degani, H. Choset, and M. T. Mason, "DSAC – Dynamic, single actuated climber: Local stability and bifurcations," in *Proc. IEEE Int. Conf. Robot. Autom.*, May. 2010, pp. 2803–2809.
[4] A. Degani, A. Shapiro, H. Choset, and M. T. Mason, "A dynamic single actuator vertical climbing robot," in *Proc. IEEE/RSJ Int. Conf. Intell. Robots Syst.*, Oct. 2007, pp. 2901–2906.
[5] A. Degani, S. Feng, H. B. Brown, K. M. Lynch, H. Choset, and M. T. Mason, "The ParkourBot— A dynamic bowleg climbing robot," in *Proc. IEEE Int. Conf. Robot. Autom.*, May 2011, pp. 795–801.
[6] A. Long, R. Gregg, and K. Lynch, "The simplest parkour model: Experimental validation and stability analysis," presented at the 14th Int. Conf. Climbing Walking Robots, Paris, France, Sep. 2011.
[7] M. H. Raibert and H. B. Brown Jr., "Experiments in balance with a 2-D one-legged hopping machine," *ASME J. Dyn. Syst., Meas., Control*, vol. 106, pp. 75–81, 1984.
[8] M. H. Raibert, H. B. Brown, and Jr, M. Chepponis, "Experiments in balance with a 3-D one-legged hopping machine," *Int. J. Robot. Res.*, vol. 3, pp. 75–92, 1984.
[9] G. Zeglin and H. B. Brown Jr., "Control of a Bow Leg hopping robot," in *Proc. IEEE Int. Conf. Robot. Autom.*, May 1998, pp. 793–798.
[10] M. H. Raibert, *Legged Robots That Balance*. Cambridge, MA, USA: MIT Press, 1986.
[11] R. Blickhan, "The spring-mass model for running and hopping," *J. Biomech.*, vol. 22, pp. 1217–1227, 1989.
[12] R. Blickhan and R. J. Full, "Similarity in multilegged locomotion: Bouncing like a monopode," *J. Comparat. Physiol.*, vol. 173, pp. 509–517, 1993.
[13] J. Schmitt and P. Holmes, "Mechanical models for insect locomotion: Dynamics and stability in the horizontal plane—I. Theory," *Biolog. Cybern.*, vol. 83, no. 6, pp. 501–515, 2000.
[14] J. Schmitt and P. Holmes, "Mechanical models for insect locomotion: Dynamics and stability in the horizontal plane—II. Application," *Biolog. Cybern.*, vol. 83, pp. 517–527, 2000.
[15] O. Arslan and U. Saranli, "Reactive planning and control of planar spring-mass running on rough terrain," *IEEE Trans. Robot.*, vol. 28, no. 3, pp. 567–579, Jun. 2012.
[16] T. Yamanaka, S. Nakaura, and M. Sampei, "Hopping motion analysis of 'superball'-like spherical robot based on feedback control," in *Proc. IEEE/RSJ Int. Conf. Intell. Robots Syst.*, 2003, pp. 3805–3810.
[17] M. Garcia, A. Chatterjee, A. Ruina, and M. Coleman, "The simplest walking model: Stability, complexity, and scaling," *J. Biomech. Eng.*, vol. 120, no. 2, pp. 281–288, Apr. 1998.
[18] A. D. Kuo, "Energetics of actively powered locomotion using the simplest walking model," *J. Biomech. Eng.*, vol. 124, no. 1, pp. 113–120, Feb. 2002.
[19] U. Saranli, M. Bühler, and D. E. Koditschek, "RHex: A simple and highly mobile hexapod robot," *Int. J. Robot. Res.*, vol. 20, no. 7, pp. 616–631, 2001.
[20] T. Allen, R. D. Quinn, R. J. Bachmann, and R. E. Ritzman, "Abstracted biological principles applied with reduced actuation improve mobility of legged vehicles," in *Proc. IEEE/RSJ Int. Conf. Intell. Robots Syst.*, 2003, pp. 1370–1375.
[21] S. A. Bailey, J. G. Cham, M. R. Cutkosky, and R. J. Full, "Comparing the locomotion dynamics of the cockroach and a shape deposition manufactured biomimetic hexapod," in *Experimental Robotics* VII (Lecture Notes in Control and Information Sciences). New York, NY, USA: Springer-Verlag, 2001, pp. 239–248.
[22] D. Longo and G. Muscato, "The Alicia^3 climbing robot: A three-module robot for automatic wall inspection," *IEEE Robot. Autom. Mag.*, vol. 13, no. 1, pp. 42–50, Mar. 2006.
[23] A. Shapiro, E. Rimon, and S. Shoval, "PCG: A foothold selection algorithm for spider robot locomotion in 2-D tunnels," *Int. J. Robot. Res.*, vol. 24, no. 10, pp. 823–844, 2005.
[24] A. Greenfield, A. A. Rizzi, and H. Choset, "Dynamic ambiguities in frictional rigid-body systems with application to climbing via bracing," in *Proc. IEEE Int. Conf. Robot. Autom.*, Barcelona, Spain, Apr. 2005, pp. 1947–1952.

[25] T. Bretl, "Motion planning of multi-limbed robots subject to equilibrium constraints: The free-climbing robot problem," *Int. J. Robot. Res.*, vol. 25, no. 4, pp. 317–342, 2006.
[26] S. Kim, M. Spenko, S. Trujillo, B. Heyneman, V. Mattoli, and M. R. Cutkosky, "Whole body adhesion: Hierarchical, directional and distributed control of adhesive forces for a climbing robot," in *Proc. IEEE Int. Conf. Robot. Autom.*, 2007, pp. 1268–1273.
[27] M. Murphy and M. Sitti, "Waalbot: An agile small-scale wall climbing robot utilizing pressure sensitive adhesives," *IEEE/ASME Trans. Mechatronics*, vol. 12, no. 3, pp. 330–338, Jun. 2007.
[28] K. Autumn, M. Buehler, M. Cutkosky, R. Fearing, R. J. Full, D. Goldman, R. Groff, W. Provancher, A. A. Rizzi, U. Saranli, A. Saunders, and D. E. Koditschek, "Robotics in scansorial environments," in *Proc. SPIE Vol. 5804 Unmanned Ground Veh. Technol. VII*, Jun. 2005, pp. 291–302.
[29] S. Kim, A. T. Asbeck, M. R. Cutkosky, and W. R. Provancher, "SpinybotII: Climbing hard walls with compliant microspines," in *Proc. 12th Int. Conf. Robot. (ICAR'05)*, Seattle, WA, USA, 2005, pp. 601–606.
[30] J. Clark, D. Goldman, P. Lin, G. Lynch, T. Chen, H. Komsuoglu, R. Full, and D. Koditschek, "Design of a bio-inspired dynamical vertical climbing robot," in *Proc. Robots: Science and Systems*, Atlanta, GA, USA, Jun. 2007.
[31] W. Provancher, S. Jensen-Segal, and M. Fehlberg, "ROCR: An energy-efficient dynamic wall-climbing robot," *IEEE/ASME Trans. Mechatronics*, vol. 16, no. 5, pp. 897–906, Oct. 2011.
[32] J. Schmitt and S. Bonnono, "Dynamics and stability of lateral plane locomotion on inclines," *J. Theor. Biol.*, vol. 261, pp. 598–609, 2009.
[33] H. B. Brown, Jr., G. Zeglin, and I. R. Nourbakhsh, "Resilient leg design for hopping running and walking machines," U.S. Patent, 7 270 589 B1, Sep. 2007.
[34] J. S. Moon and M. W. Spong, "Classification of periodic and chaotic passive limit cycles for a compass-gait biped with gait asymmetries," *Robotica*, vol. 29, pp. 967–974, 2011.
[35] R. D. Gregg, Y. Dhaher, A. Degani, and K. M. Lynch, "On the mechanics of functional asymmetry in bipedal walking," *IEEE Trans. Biomed. Eng.*, vol. 59, no. 5, pp. 1310–1318, May 2012.
[36] K. Byl and R. Tedrake, "Metastable walking machines," *Int. J. Robot. Res.*, vol. 28, no. 8, pp. 1040–1064, 2009.
[37] A. Long, A. Degani, and K. Lynch, "Feedback control experiments with the ParkourBot," in *Proc. 15th Int. Conf. Climb. Walk. Robots*, Jul. 2012, pp. 409–416.

Amir Degani (M'06) received the B.Sc. degree in mechanical engineering from the Technion—Israel Institute of Technology, Haifa, Israel, in 2002 and the M.S. and Ph.D. degrees in robotics from Carnegie Mellon University, Pittsburgh, PA, USA, in 2006 and 2010, respectively.

Since 2011, he has been an Assistant Professor with the Faculty of Civil and Environmental Engineering, Technion —Israel Institute of Technology. He is also the Director of the Civil, Environmental and Agricultural (CEAR) Laboratory. He has five pending patents in the medical robotics field. His research interests include mechanism analysis, synthesis, and design with emphasis on minimalistic concepts and the study of nonlinear dynamic hybrid systems.

Prof. Degani received the Best Paper Award at the IEEE BioRob Conference in 2006 and the Best Video Award at the IEEE ICRA Conference in 2010.

Andrew W. Long received the B.S. and the M.S. degrees in mechanical engineering from Northwestern University, Evanston, IL, USA, in 2009 and 2011, respectively. He is currently working toward the Ph.D. degree in biomedical engineering from Johns Hopkins University, Baltimore, MD, USA.

His research interests include studying motor learning and rehabilitation, specifically in the area of human locomotion.

Mr. Long received the National Defense Science and Engineering Graduate fellowship, the National Science Foundation Honorable Mention, and the Best Technical Paper Award at the International Conference on Climbing and Walking Robots in 2011.

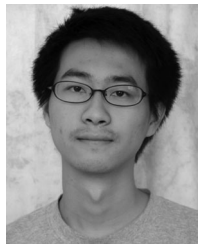

Siyuan Feng received the B.S. degree in computer science from Carnegie Mellon University, Pittsburgh, PA, USA, in 2010, where he is currently working toward the Ph.D. degree from the Robotics Institute.

He is interested in using optimization and learning techniques to generate complex robot behaviors.

Mr. Feng received the Best Video Award at the IEEE International Conference on Robotics and Automation Conference in 2010.

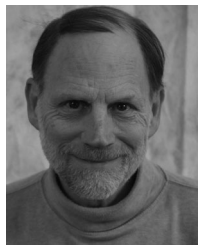

H. Benjamin Brown received the B.S. and M.S. degrees in mechanical engineering from Carnegie Mellon University, Pittsburgh, PA, USA, in 1967 and 1976, respectively.

He is a Project Scientist with the Robotics Institute, Carnegie Mellon University, Pittsburgh, PA, USA, with 30 years of experience in the robotics field. He is interested in the design and construction of robots and electro-mechanical systems and specializes in the development of high-performance structures and mechanisms, dynamically stabilized robots in particular. He has worked on a wide variety of robotics projects, including wheeled, tracked, and legged vehicles, as well as snake-like devices, for space and terrestrial applications. Recently, he has been involved in the conversion of automobiles to electric power. He has three patents and has authored or co-authored approximately 50 conference and journal papers, mainly in the field of mobile robotics.

Robert D. Gregg (M'08) received the B.S. degree in electrical engineering and computer sciences from the University of California, Berkeley, CA, USA, in 2006 and the M.S. and Ph.D. degrees in electrical and computer engineering from the University of Illinois at Urbana-Champaign, Urbana, IL, USA, in 2007 and 2010, respectively.

He is currently an Assistant Professor of mechanical engineering and bioengineering with the University of Texas at Dallas, Richardson, TX, USA. He was previously a Research Scientist with the Rehabilitation Institute of Chicago and a Postdoctoral Fellow with Northwestern University. His research interests include the control mechanisms of bipedal locomotion with application to both wearable and autonomous robots.

Dr. Gregg received the the National Institutes of Health Directors New Innovator Award and the Burroughs Wellcome Funds Career Award at the Scientific Interface. He also received the Best Technical Paper Award at the International Conference on Climbing and Walking Robots Conference in 2011, the O. Hugo Schuck Award of the IFAC American Automatic Control Council in 2009, and the Best Student Paper Award at the American Control Conference in 2008.

Howie Choset (M'94) received the Ph.D. degree in mechanical engineering from the California Institute of Technology, Pasadena, CA, USA, in 1996.

He is currently a Professor of robotics with Carnegie Mellon University, Pittsburgh, PA, USA. Motivated by applications in confined spaces, he has created a comprehensive program in snake robots, which has led to basic research in mechanism design, path planning, motion planning, and estimation. He directs the Undergraduate Robotics Minor at Carnegie Mellon University. In 2005, he co-founded Medrobotics, a company that makes a small surgical snake robot. He is the author of the book *Principles of Robot Motion* (Cambridge, MA, USA: MIT Press, 2005).

Dr. Choset won the Best Paper at the IEEE International Conference on Biomedical Robotics and Biomechatronics in 2006 and the Best video at the IEEE International Conference on Robotics and Automation (ICRA) in 2010. His students won Best Paper awards at the RIA in 1999 and at the IEEE International Conference on Robotics and Automation in 2003. In 2002, the *MIT Technology Review* elected him as one of its Top 100 Innovators in the World Under 35.

Matthew T. Mason (F'00) received the B.S., M.S., and Ph.D. degrees in computer science and artificial intelligence from The Massachusetts Institute of Technology receiving the Ph.D. degree in 1982.

Since 1982, he has been on the faculty at Carnegie Mellon University, Pittsburgh, PA, USA, where he is presently a Professor of computer science and robotics. In July 2004, became the Director with the Robotics Institute. His research interests include robotic manipulation, mobile robot error recovery, mobile robots, and robotic origami. He is the Co-Author of *Robot Hands and the Mechanics of Manipulation* (Cambridge, MA, USA: MIT Press, 1985), Co-Editor of *Robot Motion: Planning and Control* (Cambridge, MA, USA: MIT Press, 1982), and the author of *Mechanics of Robotic Manipulation* (Cambridge, MA, USA: MIT Press, 2001).

Dr. Mason received the 2009 IEEE Pioneer Award. He was a National Science Foundation Fellow from 1976 to 1980, has been an AAAI Fellow since 1992, and won the System Development Foundation Prize in 1983.

Kevin M. Lynch (F'10) received the B.S.E. degree in electrical engineering from Princeton University, Princeton, NJ, USA, and the Ph.D. degree in robotics from Carnegie Mellon University, Pittsburgh, PA, USA.

He is currently a Professor and Chair of mechanical engineering, and a member of the Neuroscience and Robotics Lab, McCormick School of Engineering and Applied Science, Northwestern University, Evanston, IL, USA. His research interests include robot manipulation and locomotion, self-organizing multiagent systems, bioinspired sensing and control, and functional electrical stimulation for restoration of human function. He is a Senior Editor of the IEEE TRANSACTIONS ON AUTOMATION SCIENCE AND ENGINEERING and co-author of *The Principles of Robot Motion*(Cambridge, MA, USA: MIT Press, 2005).

Dr. Lynch was a member of the DARPA Defense Science Study Group. He received the 2001 IEEE Early Career Award in Robotics and Automation, Northwestern's Professorship of Teaching Excellence, and the Engineering Teacher of the Year Award.